



SPE 100068

## Fatigue Integrity Analysis of Rotating Coiled Tubing

Steven M. Tipton, Gregory H. Carlson, James. R. Sorem, Jr., The University of Tulsa

Copyright 2006, Society of Petroleum Engineers

This paper was prepared for presentation at the 2006 SPE/ICoTA Coiled Tubing and Well Intervention Conference and Exhibition held in The Woodlands, TX, U.S.A., 4–5 April 2006.

This paper was selected for presentation by an SPE Program Committee following review of information contained in a proposal submitted by the author(s). Contents of the paper, as presented, have not been reviewed by the Society of Petroleum Engineers and are subject to correction by the author(s). The material, as presented, does not necessarily reflect any position of the Society of Petroleum Engineers, its officers, or members. Papers presented at SPE meetings are subject to publication review by Editorial Committees of the Society of Petroleum Engineers. Electronic reproduction, distribution, or storage of any part of this paper for commercial purposes without the written consent of the Society of Petroleum Engineers is prohibited. Permission to reproduce in print is restricted to an abstract of not more than 300 words; illustrations may not be copied. The abstract must contain conspicuous acknowledgment of where and by whom the paper was presented. Write Librarian, SPE, P.O. Box 833836, Richardson, TX 75083-3836, U.S.A., fax 01-972-952-9435.

### Abstract

By virtue of routine use, coiled tubing endures severe above-ground bending and straightening cycles that cause low-cycle fatigue to be the predominant factor limiting its useful life. For conventional coiled tubing (CT), downhole bending events associated with wellpath curvature are negligible since they are orders of magnitude less severe than above-ground cyclic bending, and applied with a very low cycle count.

A new drilling rig is under development that rotates CT at rates on the order of 20 RPM resulting in numerous operational benefits. However, rotation will impose additional rotating-bending events in the high-cycle regime as sections of tubing pass through regions of high dog leg severity. This paper presents a study of the influence of rotation on the fatigue durability of CT. In this study, fatigue data taken in the high and low cycle regimes from a variety of sources are used to assess the potential high-cycle fatigue damage that may be caused by rotation. The results indicate that the damage is below the endurance limit and thus negligible relative to conventional damage accumulated from above-ground bend-straighten cycles. This analysis also took into account another area of potential concern: circumferential abrasion that could occur when rotating coiled tubing contacts with the casing and/or wellbore. Surface roughness factors were estimated and used to modify life estimates. Results still indicate that sub-surface rotation cycles should not detrimentally influence fatigue life relative to above surface events.

Experimental results are presented which validate the conservatism of the assumptions made for surface roughness factors. The results also demonstrate that the abrasion process causes compressive residual surface stresses that somewhat offset the detrimental effect of a rougher surface.

### Introduction

Coiled tubing endures cyclic bending strains on the order of 2–3% during normal use when it moves off and back onto its deployment reel. Conventional coiled tubing units impose two

additional bend-straighten cycles when the tubing passes over the tubing guide arch (gooseneck) on its way into and out of the injectors. The rotating coiled tubing unit under development eliminates the gooseneck and thus the fatigue damage associated with it.

Conventional coiled tubing life prediction routines can predict the fatigue damage imposed by cycling off and on the spool, but none are suitable for directly assessing fatigue damage caused by the downhole rotating-bending stresses imposed on the tubing while drilling directional wells. No model has been developed for this to date because (a) even the most severe downhole curvatures are mild compared to the bending curvatures imposed by the spool and gooseneck, (b) the number of downhole cycles experienced during a typical trip is very small with non-rotating tubing and (c) coiled tubing has never been rotated downhole by conventional deployment units.

A unit that rotates CT on the order of 20 RPM could induce a large number (hundreds to thousands) of fully-reversed rotating-bending cycles on each section of tubing as it passes through regions of downhole curvature. The effect of these bending cycles relative to the fatigue damage caused above ground is the subject of this paper. To assess this effect, low-cycle fatigue data taken from strain-controlled testing [1,2] are used to estimate fatigue damage imposed by rotating bending by extrapolating into the high-cycle regime.

Another concern with rotating coil tubing downhole is the potential for circumferential surface abrasion caused by contact with the casing and/or wellbore. The additional surface roughness caused by this contact could, in theory, adversely affect fatigue damage development. Standard empirical surface roughness factors are used to assess this influence analytically.

To validate the assumptions made in this analysis, an experimental study is described. Data from full body tubes in rotational bending were collected on polished samples and samples with varying degrees of circumferential abrasion. Also, small coupon samples were used to collect additional rotating-bending fatigue data in the high cycle regime.

### Downhole Fatigue Loading

When a tube is constrained to lie in a circular arc, bending strains are imposed on its outermost surface elements equal to

$$\varepsilon = \frac{D}{2R} \quad (1)$$

where D = tubing outer diameter and R = radius of curvature of tubing centerline. This is depicted in Fig. 1 for tubing

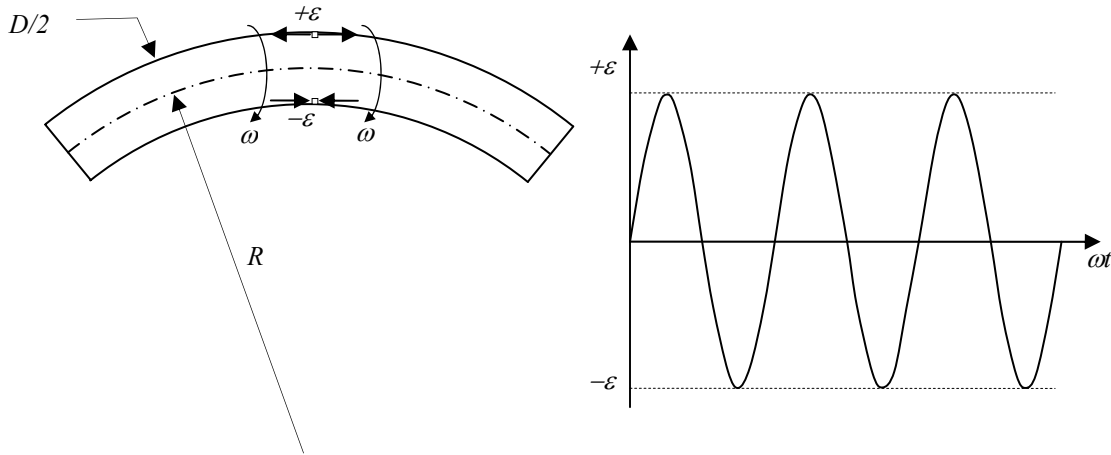


Fig. 1 - Bending strains imposed on curved section of tubing.

rotating with an angular velocity,  $\omega$ .

As the tubing rotates the strain on every surface element around the circumference fluctuates sinusoidally from  $+\epsilon$  to  $-\epsilon$ , as depicted in Fig. 1. Downhole, the dogleg severity of the well can be used to determine the local radius of curvature (R) as shown in Fig. 2.

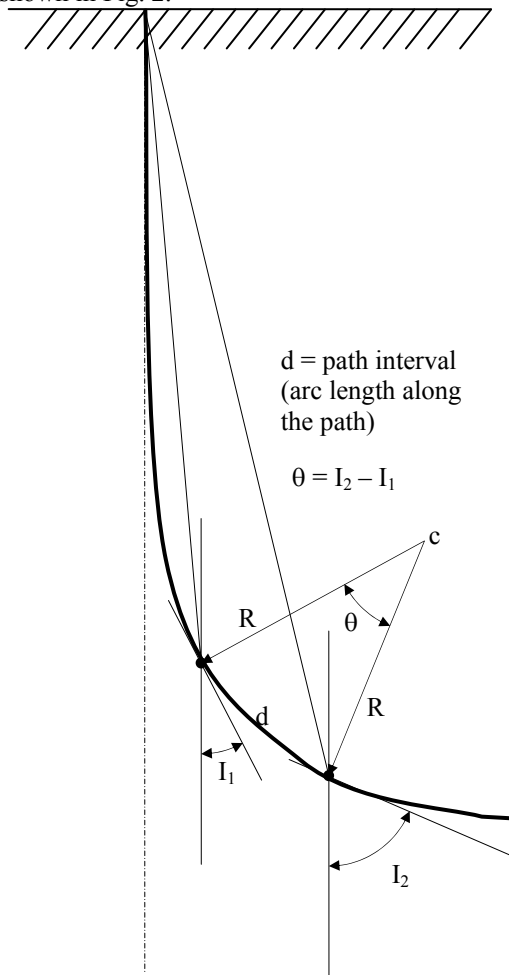


Fig. 2 - Dogleg severity associated with a downhole well path.

From Fig. 2, DLS is defined as the angular change in the wellpath tangent,  $\theta$ , per length along the wellpath of length,  $d$ , as given in Eqn. 2.

$$DLS = \frac{\theta}{d} \tag{2}$$

or, since DLS values are typically expressed in degrees per 100 ft,

$$\theta = DLS(100\text{ ft}) \frac{\pi}{180^\circ} \tag{3}$$

The “100ft” terms essentially cancel out, and the angular expression for DLS can also be considered the angle,  $\theta$ , corresponding to a circular arc of length of 100ft occurring with a uniform radius of curvature, R. Therefore,

$$R = \frac{100\text{ ft}}{\theta} \tag{4}$$

For example, for a DLS of 25°/100ft, R is given by

$$R = \frac{100\text{ ft}}{(25^\circ / 100\text{ ft})(100\text{ ft } \pi / 180^\circ)} = 229.2\text{ ft} \tag{5}$$

In accordance with Eqn. 1, this curvature would induce a maximum bending strain of 0.00059, or 0.059% at the outer surface of 3.25” diameter coiled tubing.

The highest values of DLS encountered in actual directional wells are on the order of 25°/100ft, although localized values as high as 45°/100ft are sometimes associated with milled windows at kick-offs or ultra short radius drilling. Such high DLS values are not anticipated for the rotating system under consideration here.

**Fatigue Life Prediction Data and Equations**

For the rotating rig in this study, DLS values greater than 25°/100ft are rarely expected to occur. As mentioned previously, this corresponds to a radius of curvature of 229 ft or 2,750 inches and causes a fully-reversed maximum bending strain amplitude of 0.00059 at the outer surface. However, experience has shown that fatigue lives taken from coupon samples tested in axial strain-controlled loading, more closely correlate with the average flexural strains in the tube wall. Due to the linear distribution of bending strains, the average strain in the wall of tubing with a thickness of  $t$  is given by Eqn. (6).

$$\epsilon = \frac{(D-t)}{2R} \tag{6}$$

For  $t = 0.25$ ” (HS90 3.25” OD, 0.25” wall thickness coil), this corresponds to a fluctuating strain amplitude of  $\epsilon_a = 0.000545$ .

For fully reversed loading, the strain amplitude is related to fatigue life by the Manson-Coffin [3,4] relation:

$$\varepsilon_a = \frac{\sigma_f'}{E} (2N)^b + \varepsilon_f' (2N)^c \quad (7)$$

The constants,

- $\sigma_f'$  = fatigue strength coefficient
- b = fatigue strength exponent
- $\varepsilon_f'$  = fatigue ductility coefficient
- c = fatigue ductility exponent

were obtained for coiled tubing material from strain controlled fatigue testing as per ASTM E606, as described in [1] For each material, Eqn. 7 was fit through the data to define the constants, which are considered fatigue properties for that particular alloy. It is important to note that the smallest strain range used to collect data from the axial coupon samples was 0.003 (0.3%). This corresponds to lives on the order of 4000-8000 cycles. Although these lives are much higher than the regime in which coiled tubing normally operates, they are well below the range associated with damage induced by subsurface rotating-bending. However, the parameters were formulated with extrapolation into the high-cycle regime taken closely into consideration. Individual alloys were fit such that strain ranges associated with lives of  $10^6$  were estimated with reasonable conservatism relative to other coiled tubing alloys, and other steel alloys with similar tensile properties.

To account for residual mean stresses,  $\sigma_m$ , the Manson-Halford [5] equation can be used, as given in Eqn. 8.

$$\varepsilon_a = \frac{\sigma_f' - \sigma_m}{E} (2N)^b + \varepsilon_f' \left( \frac{\sigma_f' - \sigma_m}{\sigma_f'} \right)^{c/b} (2N)^c \quad (8)$$

where the mean stress,  $\sigma_m$ , can be approximated based on analysis of the elastoplastic cyclic stress-strain state in the walls of the tubing. Factors such as cyclic stress relaxation are accounted for implicitly in such an analysis by using the cyclic stress-strain parameters,  $K'$  and  $n'$  (the cyclic strength coefficient and cyclic strain hardening exponent, respectively) via the Ramberg-Osgood [6] relations,

$$\varepsilon_a = \frac{\sigma_a}{E} + \left( \frac{\sigma_a}{K} \right)^{1/n'} \quad (9)$$

along with a Massing [7,8] assumption to account for load reversals.

### Surface Roughness Factors

Since the surface of coiled tubing may be scored by contact with the wellbore during rotation, the potential exists for this additional surface roughness to affect the fatigue life. This influence has been observed to affect the high-cycle portion of the strain-life relation. Therefore, a surface roughness factor,  $k_s$ , is used to modify the fatigue strength exponent as follows. The cycle count associated with the endurance limit in smooth material,  $S_e$ , is  $N_e$ .  $S_e$  is computed by  $\sigma_f' (2N_e)^b$ . The reduced fatigue strength exponent,  $b_s$ , is computed by:

$$b_s = - \frac{\log \left( \frac{\sigma_f'}{k_s S_e} \right)}{\log(2N_e)} \quad (10)$$

The modified fatigue strength exponent is used in Eqns. 7 or 8 in place of b to account for surface roughness without or with a mean stress, respectively [8].

### Life Estimates for Downhole Rotating Bending

The equations defined in the previous section were used to estimate fatigue damage caused by high cycle fatigue (HCF) loading. Although the strain in the walls of coiled tubing due to flexure cycling on the spool ranges from zero in the straight position to maximum given by Eqn. 6 when bent, the stress state is essentially completely reversed. As much bending stress is required to return the strain to zero during straightening as was required to apply the plastic strain during bending.

The rotating stresses downhole should mitigate the residual stresses in the tube walls, which have already been relaxed somewhat due to the straightener above the injector. Analysis using the cyclic stress-strain relation, Eqn. 9, conservatively estimates the magnitude of the mean stress to lie between 10 and 20% of the cyclic yield strength.

The anticipated DLS window for wells drilled with the rotary unit is 5-15°/100ft, with a maximum of 25°/100ft. The maximum value causes curvature of  $R = 2,750$ in, which imposes an average bending strain range of 0.000545 from Eqn. 6 for 3.25" diameter tubing with a wall thickness of 0.25". Using a 90 ksi material, the following life predictions can be made by Eqns. 7 and 8 without and with mean stress correction.

To account for surface roughness, a *very* conservative estimate of the endurance limit of  $k_s = 0.6$  can be assumed, based on surfaces resulting from conventional drillpipe used for directional drilling applications.

Using surface roughness factors of 0 (smooth) and 0.6 (rough) and mean stresses of 0 and 0.2 x cyclic yield stress (= 0.2 (68 ksi) = 13.6 ksi), the life predictions for HS90 3.25" x 0.25" tubing rotating with a DLS = 25°/100ft are presented in the Table 1.

**Table 1 – Life Estimates for Limiting Values of  $\sigma_m$  and  $k_s$**

	Life Estimate (cycles)	
	$k_s = 0$	$k_s = 0.6$
$\sigma_m = 0$	102,866,660	2,151,423
$\sigma_m = 0.2S_y'$	59,155,134	1,386,299

The most important point about these estimates is that they all exceed the life of  $10^6$ , associated with the endurance limit for this material. (Even with the most conservative estimates for surface roughness and mean stress.) For practical purposes, this means the cycles endured at this level *make no contribution to fatigue damage*. Therefore, conventional coiled tubing life prediction routines that only consider the fatigue damage imposed above surface should be adequate to monitor the service life of rotating coiled tubing in the field. The curve used to make these predictions was generated at maximum lives of only about 8000 cycles. However, the strain life curve (Eqn. 7) was extrapolated into the high cycle regime with additional conservatism, manifested by the formulation of the constants  $\sigma_f'$  and b.

Additional conservatism is incorporated into these life estimates by use of a surface roughness factor of 0.6. Surface conditions corresponding to directional drillpipe are assumed

to lie in a range from 80 to 120  $\mu\text{in}$  rms. For this range, surface roughness factors,  $k_s$ , are more reasonably expected to lie in a range from 0.9 to 0.85 [9]. Furthermore, research results [10,11] on rotating bending fatigue samples of low carbon steels have indicated that a circumferentially abraded surface finish on the order of 20-25  $\mu\text{in}$  rms lowered fatigue life in the endurance limit regime by a factor of  $k_s = 0.91$  relative to a polished surface with a roughness of 4-5  $\mu\text{in}$  rms. However, surfaces that were abraded circumferentially to a rougher range of 70-80  $\mu\text{in}$  rms actually showed **an improved fatigue life**. This behavior was explained by residual compressive stresses acting perpendicular to the direction of the circumferential grinding marks.

This hypothesis was validated by subsequent tests run on samples that had been stress-relief annealed to remove the residual stresses and those samples showed a reduced life for all surface roughness, relative to the polished and ground surfaces. What this means to rotating coiled tubing is that any fatigue life reduction that could be expected from circumferential abrasion could potentially be offset by residual stresses induced in the rougher surface. Neglecting this fact adds additional conservatism to the predictions presented in the table above.

### Experimental Studies

In order to evaluate the assumptions about surface roughness factors used in this analysis and to address the issue of residual compressive stress influence, two sets of rotating-bending (RB) fatigue experiments were conducted.

One set involved testing 1.25" diameter tubular samples of 90 ksi grade coiled tubing. The samples were loaded in RB using the machine depicted in Fig. 3. As shown in Fig. 3, a gauge section of reduced wall thickness was machined into the middle of the samples. This was necessary to avoid grip-related failures. Samples were tested with a polished surface, and with surfaces circumferentially abraded by medium and rough emery cloth. The other data set was generated using small 1/2 inch diameter coupon samples, shown in Fig. 4.

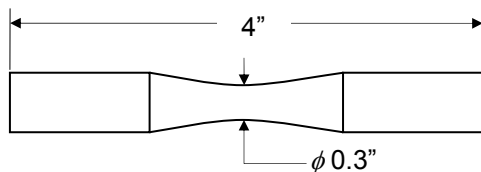


Fig. 4 - Small rotating-bending coupon sample geometry.

The alloy used for these samples was hot rolled 4130 steel. The strength and hardness of this alloy are similar to the

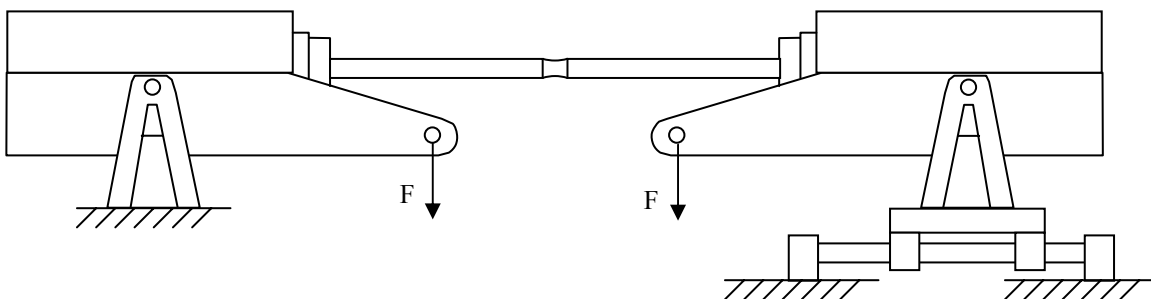


Fig. 3 - Schematic illustration of 4-point bending machine used to test 1.25" coiled tubing samples.

modified A606 alloy used to manufacture the 90 ksi grade of coiled tubing.

The small coupon sample surfaces were prepared using the following procedure.

- Set A was polished longitudinally until all circumferential machining marks were removed.
- Set B was roughened using 120 grit emery cloth held on a sample while rotating in a lathe for about 15 seconds to induce a "fine" surface finish.
- Set C was roughened using 100 grit emery cloth to induce a "medium" surface finish
- Set D was roughened using 40 grit emery cloth to induce a "coarse" surface.

Table 2 below shows the average surface roughness associated with the samples sets:

Table 2 – Coupon RB surface Preparation

Surface Condition	Cloth Grit	Ra roughness
A – Polished	N/A	3.4 $\mu\text{in}$
B – Fine	120	24.3 $\mu\text{in}$
C – Medium	100	57.5 $\mu\text{in}$
D – Coarse	40	78.8 $\mu\text{in}$

Initially, half of the samples were prepared in this manner and the other half were left in the "as machined" condition. All samples were then stress relief annealed by heating in a vacuum to 1150 °F, holding for 1 hour, then oven cooling to ambient temperature. After all samples were heat treated, the "as machined" samples were prepared identically to sets B, C and D, to produce sets B<sub>r</sub>, C<sub>r</sub> and D<sub>r</sub>. The subscript, r, indicates that the residual stresses were **not** eliminated from these samples. Note that all polished samples were polished prior to heat treating, to remove residual stresses from the baseline samples. It should be noted that the hardness was measured before and after the stress relief procedure, and no changes were noted (93 R<sub>b</sub>). The microstructure was also observed to be unaffected by the heat treatment.

### Full Body Tube RB Fatigue Results

The fatigue data from the 1.25" full body tubular samples are shown in Fig. 5.

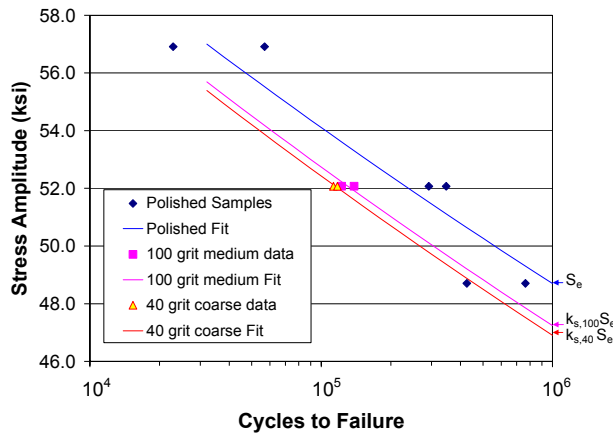


**Fig. 5 – Fatigue data for full tubes in rotating-bending. Polished sample data were taken at 3 load levels, and abraded surface data were taken at only one load level.**

As Fig. 3 illustrates, it was necessary to machine a section of reduced wall thickness in the center of the sample. Several attempts were made to generate fatigue failures without such a reduced section, but the samples always failed at the stress concentration associated with the grip. The tubing samples were made from 1.25-inch HS90 material with a 0.095 nominal wall thickness that was actually about 0.103 in. The minimum diameter in the reduced section was 1.164 in. which reduced the wall thickness to a value of 0.060 in.

The reduced sections were roughened using two different grits of emery cloth, held against the rotating gauge sections for about 15 seconds. The grits were 100 (medium) and 40 (rough). Due to the geometry of these samples, it was not possible to measure the resulting surface roughness with the profilometer available for this study. However, an identical procedure was used on the small diameter samples and similar surfaces were induced (for Ra values of about 58 and 79  $\mu\text{in}$ ).

The polished samples were tested at three different load levels in order to roughly estimate a baseline fatigue strength coefficient and exponent,  $\sigma_f'$  and  $b$ . Using these parameters and the fatigue data point taken as the average life generated at each roughness, the reduced exponent,  $b_s$ , could also be estimated for each roughness. Using these parameters, the surface roughness factor,  $k_s$ , could be calculated from Eqn. 10, assuming an endurance limit threshold life of  $N_e = 10^6$ . From this procedure,  $k_s$  values for the medium (100 grit) and coarse (40 grit) surfaces are

$$k_{s,100} = 0.970$$

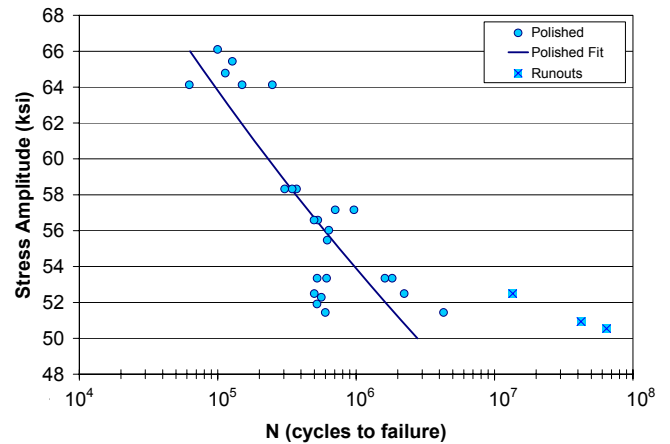
$$k_{s,40} = 0.963$$

These values agree very favorably with the values from the R.C. Johnson tables [9]. Using the minimum yield strength for this alloy of 97 ksi, the R.C. Johnson tables estimate  $k_s$  values of 0.96 and 0.97, for the 100 and 40 grit medium and coarse roughnesses, respectively.

**Small Coupon RB Fatigue Results**

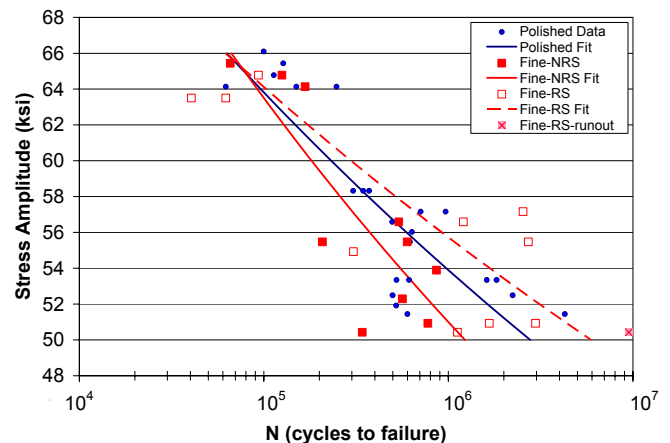
The fatigue data from the small coupon samples are presented in Figs. 6-9. The data reveal trends that are similar to those from the work of Ferguson [10,11].

Fig. 6 presents data from the baseline, polished samples.



**Fig. 6 – Fatigue data for sets A with polished surfaces.**

The scatter near the endurance limit is considerable. A group of samples failed around 500,000 cycles, while others at the same load level lasted a few million cycles, or ran out (did not fail), lasting longer than  $10^7$  cycles. Despite this scatter, a power law curve was fit through the finite-life samples as shown.



**Fig. 7 – Fatigue data for sets B (NRS) and B<sub>r</sub> (RS) with “fine” surfaces.**

In Fig. 7, the overall trend of the fine B<sub>r</sub> samples with residual stresses (RS) actually shows improved fatigue performance relative to polished baseline samples, consistent with the observations from Ferguson’s work. Without the residual stresses (NRS), the fine heat treated B samples failed slightly sooner than the polished samples, as shown by the power law curves fit through each set of data.

All medium and coarse samples in Figs. 8-9 both showed reduced fatigue strength relative to the polished samples. However, for the same roughness, samples with residual stresses (RS) showed slightly longer fatigue lives relative to stress relieved samples (NRS). These plots consistently support the hypothesis that two separate mechanisms are at work: (1) rougher surface reduced the fatigue resistance while (2) residual compressive stresses induced during the surface abrasion process improve the fatigue resistance. In the case of set B, the beneficial effect of residual compressive stress is slightly greater than the negative effect of the roughened surface.

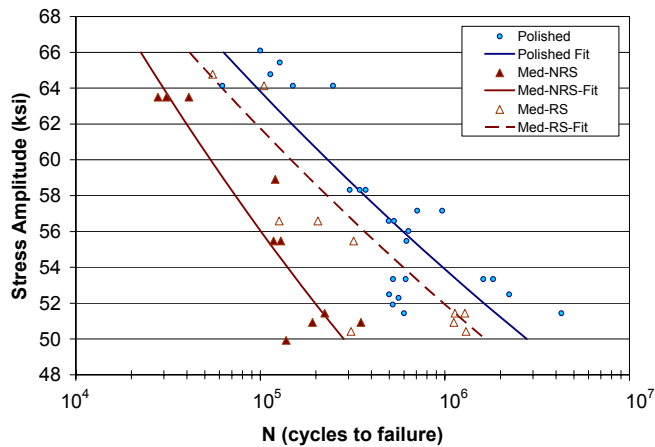


Fig. 8 – Fatigue data for sets C (NRS) and Cr (RS) with “medium” surfaces.

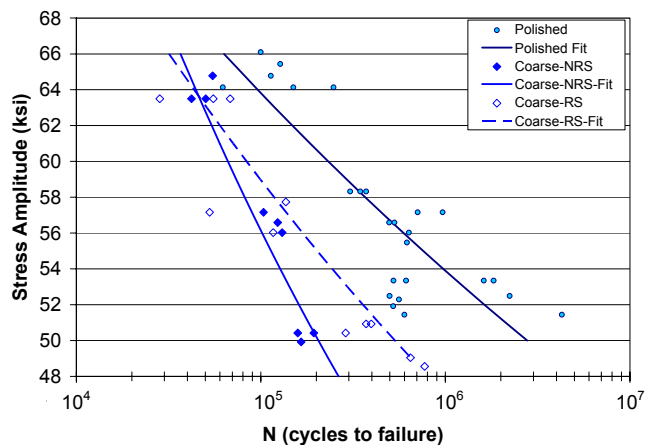


Fig. 9 – Fatigue data for sets D (NRS) and Dr (RS) with “coarse” surfaces.

## Discussion

The experimental results confirm some of the assumptions made in the analysis of downhole rotationally induced fatigue damage: The assumption of a surface roughness factor of 0.6 is extremely conservative. Coarse, 40 grit emery cloth induces a surface with an Ra of about 80  $\mu\text{m}$ , corresponding to a surface roughness factor of about  $k_s = 0.96$ . A roughness factor of  $k_s = 0.6$  corresponds to a surface with a roughness of 2000  $\mu\text{m}$ , according the R.C. Johnson curves. A surface roughness of 2000  $\mu\text{m}$  is twice as severe as a typical flame cut surface, far more severe than the abrasion experienced by downhole tool pipes during conventional rotary drilling.

The small coupon data showed fatigue life reductions similar to the full body tubes, based on data points from surfaces roughened after stress relieving (the RS data points), but lower  $k_s$  values when residual stresses were removed. Surface roughness values computed for both conditions from all three sets of data are presented in Table 3.

Table 3 – Small Coupon Surface Roughness Factors

Surface Condition	$k_s$ - RS	$k_s$ - NRS
B – Fine	>1	0.95
C - Medium	0.96	0.84
D - Coarse	0.88	0.81

The RS data for the medium roughness agrees well with the full body tube data, but the coarse surface shows a lower  $k_s$  than the full body tubes. It should be noted that the surface roughness on the full body tubes could not be measured with the instrumentation available, and could account for the 8% difference in these  $k_s$  values.

The samples abraded after stress relief exhibited a distinct beneficial effect of residual compressive surface stresses, caused by the abrasive process, as observed by Ferguson [10,11]. Although interesting, its effect is not strong enough to be relied upon for predicting additional fatigue life for rotating coiled tubing in field applications.

Due to scatter, additional fatigue data should be gathered in the high cycle regime, to facilitate the extension of coiled tubing life prediction models, such as described in Ref. [2], into the HCF regime. It is anticipated that the use of these results would only become necessary in the event dogleg severities arise that are more severe than the anticipated maximum value of 25°/100ft. In fact, based on the conservatism embedded in the preliminary analysis, additional testing would likely identify a threshold value of DLS considerably greater than 25°/100ft.

The need to apply such a HCF model to situations in the field is affected by the rate of penetration (ROP) in addition to the rotational speed (RPM). A model must compute the number of downhole cycles required to pass through a given section based on RPM and ROP and calculate fatigue damage correspondingly. For example, to pass through a 50ft section with an extremely severe DLS of 45°/100ft at an ROP of 20 ft/hr would require 3000 revolutions. Using worst case approximations of surface roughness and mean stress, this would be computed to expend approximately 5% of the tubing life for that section. Additional research in the HCF regime will refine predictions such as this.

## Conclusions

A rotating coiled tubing drilling system imposes coiled tubing rotation at a maximum rate on the order of 20 RPM for enhanced drilling performance. The additional fatigue cycling the tubing must endure as it passes through curved sections of directional wellpaths is shown to lie below the endurance limit of the 90 ksi grade of coiled tubing material. These predictions are based on very conservative estimates of material properties, surface roughness and mean stresses associated with above ground bending-straightening.

In order to quantify the conservatism of the analytical predictions, an experimental program was undertaken to generate fatigue data for coiled tubing in the high cycle regime. Full body tubular samples were loaded in rotating-bending with surfaces circumferentially roughened to varying extents. Additional HCF data were taken using small coupons of a similar alloy with varying surface roughnesses imposed by circumferential abrasion. These data validated the conservatism of the assumptions used to estimate of the effect of surface roughness of fatigue resistance. They also validated a beneficial effect of residual compressive surface stress, caused by the abrasive process itself. Although these residual stresses offset the severity of the roughened surfaces, the effect is small enough that it should not be relied upon to predict additional fatigue life in the field at this time.

Additional HCF testing is needed to facilitate the extension of current life prediction models into the regime associated with lower strain range downhole cycling. Such a model could be implemented to supplement conventional coiled tubing fatigue life prediction software for the rare occasions when downhole DLS values exceed a threshold level, also computed from research results.

### Acknowledgements

The authors would like to thank Highgate Ltd. for supporting this research. Thanks also to undergraduate laboratory technicians, Blane Rhodes, Susan Bley and Zach Penix.

### References

1. Tipton, S.M., "Low-Cycle Fatigue Testing of Tubular Material using Non-Standard Specimens," Effects of Product Quality and Design Criteria on Structural Integrity, ASTM STP 1337, R.C. Rice and D.E. Tritsch, Eds., American Society for Testing and Materials, 1998, pp. 102-119.
2. Tipton, S.M., "Multiaxial Plasticity and Fatigue Life Prediction in Coiled Tubing," *Fatigue Lifetime Predictive Techniques: 3rd Volume*, ASTM STP 1292, M.R. Mitchell and R.W. Landgraf, Eds., American Society for Testing and Materials, 1996, pp. 283-304.
3. Manson, S.S., "Behavior of Materials under Conditions of Thermal Stress," *Heat Transfer Symposium*, University of Michigan Engineering Research Institute, 1953, pp. 9-75 (also published as NACA TN 2933, 1953).
4. Coffin, L.L., Jr., "A Study of the Effects of Cyclic Thermal Stresses on a Ductile Metal," *Trans. ASME*, Vol. 76, 1954, pp. 931-950.
5. Manson, S.S. and Halford, G.R., "Practical Implementation of the Double Linear Damage Rule and Damage Curve Approach for Treating Cumulative Fatigue Damage," *International Journal of Fracture*, Vol. 17, No. 2, p. 169, 1981.
6. Ramberg, W. and Osgood, W., "Description of Stress-Strain Curves by Three Parameters," *NACA TN 902*, 1943.
7. Massing, G., "Eigenspannungen und Verfestigung beim Messing (Residual Stress and Strain Hardening of Brass)," *Proceedings, Second International Congress for Applied Mechanics, Zurich, September, 1926*.
8. Dowling, N.E., *Mechanical Behavior of Materials*, 2nd Edition, 1998.
9. Johnson, R.C., *Machine Design*, Vol. 45, No. 11, p. 108, 1973.
10. Ferguson, R.R., "Effect of Surface Finish on Fatigue Properties at Elevated Temperatures," *NACA Research Memorandum*, RM E51D17, 1951.
11. Ferguson, R.R., "A Further Investigation of the Effect of Surface Finish on Fatigue Properties at Elevated Temperatures," *NACA Technical Note*, TN3142, 1954.